ACCOUNTS of chemical research

Article

pubs.acs.org/accounts

Bioinspired Nonheme Iron Catalysts for C−H and C═C Bond Oxidation: Insights into the Nature of the Metal-Based Oxidants

Published as part of the Accounts of Chemical Research special issue "Earth Abundant Metals in Homogeneous Catalysis".

Williamson N. Oloo and Lawrence Que, Jr.*

Department of Chemistry and Center for Metals in Biocatalysis, University of Minnesota, Minneapolis, Minnesota 55455, United States

Supporting Information

CONSPECTUS: Recent efforts to design synthetic iron catalysts for the selective and efficient oxidation of C−H and C═C bonds have been inspired by a versatile family of nonheme iron oxygenases. These bioinspired nonheme (N4)Fe^{II} catalysts use H_2O_2 to oxidize substrates with high regio- and stereoselectivity, unlike in Fenton chemistry where highly reactive but unselective hydroxyl radicals are produced. In this Account, we highlight our efforts to shed light on the nature of metastable peroxo intermediates, which we have trapped at −40 °C, in the reactions of the iron catalyst with H_2O_2 under various conditions and the high-valent species derived therefrom.

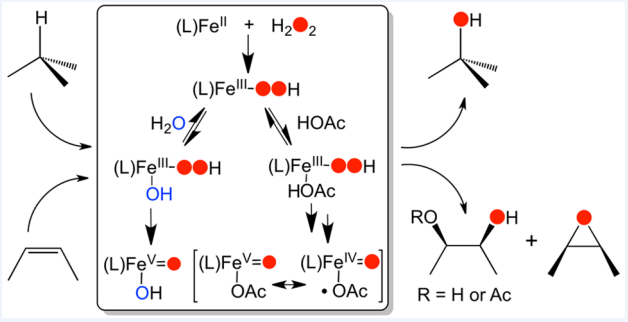

Under the reaction conditions that originally led to the discovery of this family of catalysts, we have characterized spectroscopically an Fe^{III}−OOH intermediate (EPR g_{max} = 2.19) that leads to the hydroxylation of substrate C−H bonds or the epoxidation and *cis*-dihydroxylation of C═C bonds. Surprisingly, these organic products show incorporation of ^{18}O from $H_2{}^{18}O$, thereby excluding the possibility of a direct attack of the Fe^{III}−OOH intermediate on the substrate. Instead, a water-assisted mechanism is implicated in which water binding to the iron(III) center at a site adjacent to the hydroperoxo ligand promotes heterolytic cleavage of the O−O bond to generate an Fe^{V}(O)(OH) oxidant. This mechanism is supported by recent kinetic studies showing that the Fe^{III}−OOH intermediate undergoes exponential decay at a rate enhanced by the addition of water and retarded by replacement of H_2O with D_2O, as well as mass spectral evidence for the Fe^{V}(O)(OH) species obtained by the Costas group.

The nature of the peroxo intermediate changes significantly when the reactions are carried out in the presence of carboxylic acids. Under these conditions, spectroscopic studies support the formation of a (κ^2-acylperoxo)iron(III) species (EPR g_{max} = 2.58) that decays at −40 °C in the absence of substrate to form an oxoiron(IV) byproduct, along with a carboxyl radical that readily loses CO_2. The alkyl radical thus formed either reacts with O_2 to form benzaldehyde (as in the case of $PhCH_2COOH$) or rebounds with the incipient Fe^{IV}(O) moiety to form phenol (as in the case of C_6F_5COOH). Substrate addition leads to its 2-e^- oxidation and inhibits these side reactions. The emerging mechanistic picture, supported by DFT calculations of Wang and Shaik, describes a rather flat reaction landscape in which the (κ^2-acylperoxo)iron(III) intermediate undergoes O−O bond homolysis reversibly to form an Fe^{IV}(O)($^{\bullet}OC(O)R$) species that decays to Fe^{IV}(O) and $RCO_2^{\bullet}$ or isomerizes to its Fe^{V}(O)(O_2CR) electromer, which effects substrate oxidation. Another short-lived S = 1/2 species just discovered by Talsi that has much less g-anisotropy (EPR g_{max} = 2.07) may represent either of these postulated high-valent intermediates.

INTRODUCTION

C−H and C═C bond oxidations are important transformations performed by O_2 activating mononuclear nonheme iron enzymes in key metabolic transformations.[1] These enzymes have iron active sites with a recurring 2-His-1-carboxylate facial triad motif that in many cases generates an oxoiron(IV) oxidant.[2] The Rieske-dependent oxygenases[3] are an exception within this large family in requiring NADH as a reductant, suggesting the possibility of a mechanism more akin to that of the heme enzyme cytochrome P450 (Scheme 1).[4] Crystallographic studies of naphthalene 1,2-dioxygenase (NDO)[5] and carbazole 1,9a-dioxygenase[6] show the formation of a side-on O_2 adduct that is trapped *in crystallo* when a substrate analog is present, which is presumably the precursor of the putative oxoiron(V) oxidant (Scheme 1). These two enzymes catalyze the regio- and stereospecific *cis*-dihydroxylation of substrate arene C═C bonds with the incorporation of both atoms of O_2 into the diol product (Figure 1a). More recently, Rieske-dependent enzymes have also been found that

Received: January 31, 2015
Published: August 17, 2015

DOI: 10.1021/acs.accounts.5b00053
Acc. Chem. Res. 2015, 48, 2612−2621

Scheme 1. Dioxygen Activation Mechanisms for Cytochrome P450 (top) and Rieske Oxygenases (bottom)[a]

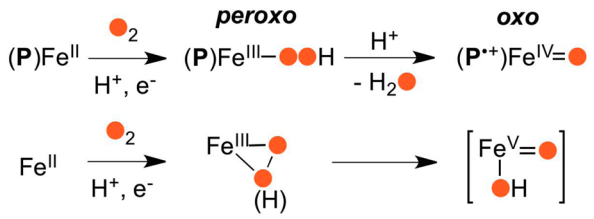

[a]P = porphyrin.

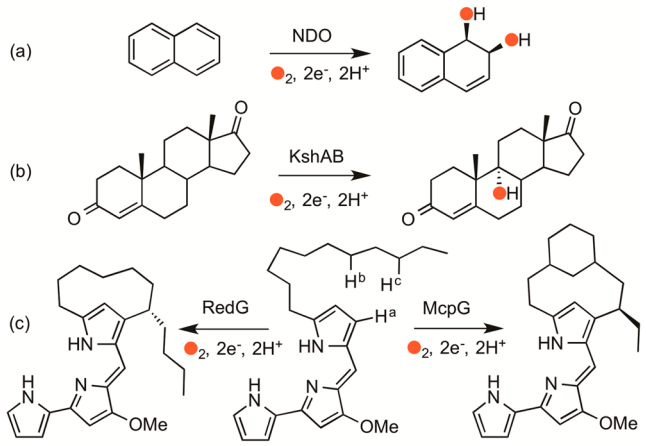

Figure 1. Examples of reactions catalyzed by Rieske oxygenases.[3]

functionalize substrate C−H bonds in cholesterol catabolism (Figure 1b) and antibiotic biosynthetic pathways (Figure 1c).[3]

Much mechanistic insight into O_2 activation by Rieske-dependent oxygenases has been obtained from studies of NDO (Figure 1a) and closely related enzymes. O_2 binding to the iron(II) center affords the crystallographically characterized Fe(η^2-O_2) adduct,[5,6] which is best described as a high-spin Fe^{III}(η^2-OOH) intermediate based on the EPR and Mössbauer characterization of an intermediate derived from the reaction of fully oxidized benzoate 1,2-dioxygenase with H_2O_2.[7] This intermediate effects a single turnover of benzoate oxidation to its *cis*-dihydrodiol product. The proposed Fe^{III}(η^2-OOH) intermediate may either oxidize substrates directly or first convert to a putative Fe^{V}(O)(OH) species electronically analogous to P450-Cpd I.[8] Indirect experimental support for the latter comes from ^{18}O-incorporation from $H_2{}^{18}O$ into the oxidation products of naphthalene (3% into the *cis*-1,2-dihydrodiol)[9] and indan (68% into 1-indanol).[10]

The marked increase in information on nonheme iron oxygenases within the last 20 years[3] has spurred efforts to develop corresponding biomimetic iron oxidation catalysts.[11] While the holy grail of finding catalysts that activate O_2 for substrate oxidation remains elusive, significant progress has been made in the use of H_2O_2 (replacing the $O_2/2e^-/2H^+$ combination) to carry out the regio- and stereoselective oxidations of C−H and C═C bonds. The main challenge in developing catalysts for H_2O_2 activation is to identify reaction conditions that minimize the production of highly reactive but unselective hydroxyl radicals[12] and instead generate a more selective high-valent metal-based oxidant, analogous to oxidants formed by the aforementioned heme and nonheme oxygenases.[11] Most of the effective iron catalysts identified thus far are supported by tetradentate N4 ligands and possess two *cis*-oriented sites on the iron center for peroxide binding and activation (Chart 1).

Chart 1. Ligands Used for Bio-Inspired Nonheme Fe^{II}(L) Catalysts in Hydrocarbon Oxidations Using H_2O_2[a]

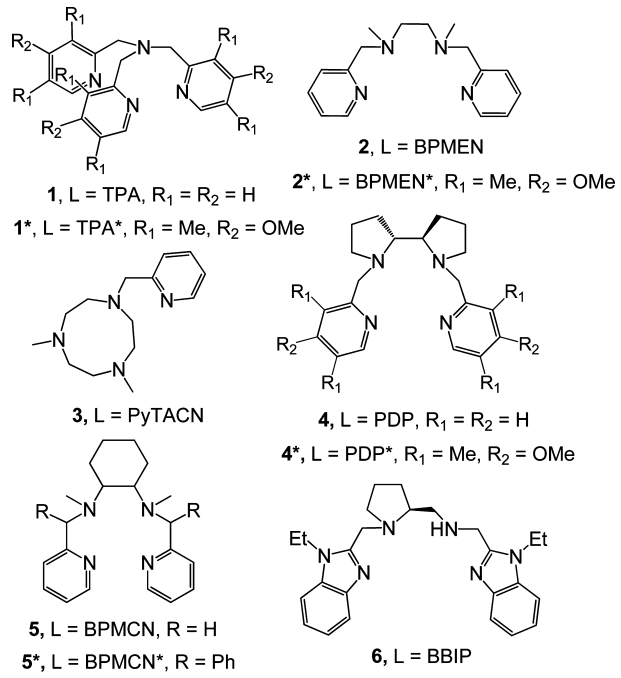

[a]The number designates the Fe^{II} complex supported by the ligand shown.

In this Account, we provide a perspective on our efforts to mimic the reactivity of nonheme oxygenases and develop iron catalysts for synthetic applications.[11] We mainly focus on the mechanistic insights obtained into how these catalysts work, so that such knowledge may be applied to the design of iron catalysts with superior efficiency and selectivity in the oxidation of C−H and C═C bonds using H_2O_2 as oxidant.

BIOINSPIRED NONHEME IRON CATALYSTS FOR C−H AND C═C BOND OXIDATIONS BY H_2O_2

We reported the first example of a nonheme iron(II) catalyst capable of the stereoselective oxidation of unactivated C−H bonds using H_2O_2 in 1997.[13] Since then, other iron complexes have been shown to exhibit similar catalytic behavior.[11,14−16] In particular, complexes **1**−**3**,[17,18] respectively, supported by TPA, BPMEN, and PyTACN ligands (Chart 1), were found to oxidize cyclohexane predominantly to the cyclohexanol product and *cis*-1,2-dimethylcyclohexane to *trans*-1,2-dimethylcyclohexanol with >93% stereoretention. Although the observed selectivity of these reactions was desirable, the main drawback was the excess substrate required to maximize the conversion of H_2O_2 into desired products. To meet this challenge, White and co-workers replaced BPMEN with PDP to afford catalyst **4**, which exhibited enhanced selectivity and afforded high product yields in the presence of AcOH additive such that excess substrate was no longer required.[19] Even more importantly, **4** enabled the oxidation reactions to be carried out with excellent and predictable selectivity for the most electron-rich and least sterically hindered tertiary C−H bonds (See Figure 2 for examples).[19,20] These iron complexes also catalyze asymmetric alkene oxidation. Replacement of BPMEN with chiral BPMCN,

DOI: 10.1021/acs.accounts.5b00053
Acc. Chem. Res. 2015, 48, 2612−2621

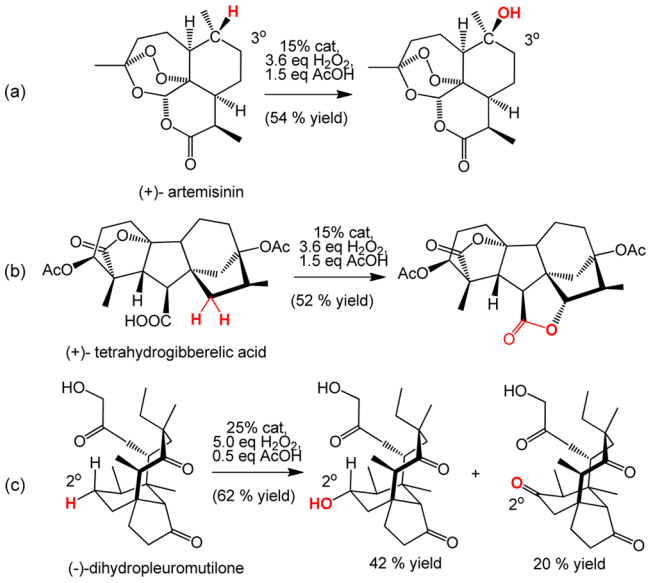

Figure 2. Examples of selective aliphatic C−H bond oxidations by **4** in natural product synthesis.[19,20]

PDP, and BBIP ligands (Chart 1) leads to high yielding epoxidation reactions with enantioselectivities as high as 99% (See Figure 3 for examples).[15,16,21]

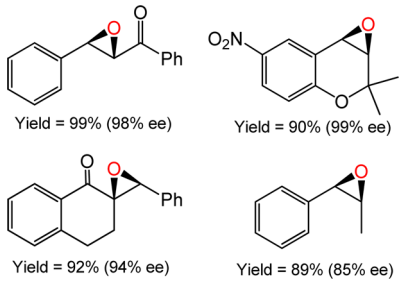

Figure 3. Examples of enantioselective olefin epoxidation by **4**, **5**, and **6** with H_2O_2.[22−25]

These results clearly demonstrate that it is possible to design efficient catalysts with predictable selectivity for the late-stage modification of C−H and C═C bonds in polyfunctional organic molecules without the need for activating and protecting groups, which is an important achievement in synthetic organic chemistry. However, there are still significant drawbacks such as high catalyst loadings and limited substrate scope. An important goal is therefore to understand the mechanistic details of these and related catalysts that will facilitate the rational design of new catalysts with superior activity and predictability.

The combination of iron(II) and H_2O_2 for oxidative transformations often raises the spectre of hydroxyl radicals as the incipient oxidants, which are highly reactive and indiscriminate and thus undesirable.[12] A much more selective metal-based oxidant is implicated by the nature of the products generated from the nonheme iron catalysts shown in Chart 1, particularly the high degree of stereoretention found in the 3°-alcohol product from *cis*-1,2-dimethylcyclohexane oxidation,[13,17,18] and in the epoxide and *cis*-diol products from olefin oxidation.[26,27] Such stereoselective transformations make it highly unlikely that hydroxyl radicals are involved.

Isotope labeling experiments provided significant early insight into the nature of this metal-based oxidant. As shown in Figure 4, label incorporation from added $H_2{}^{18}O$ is observed

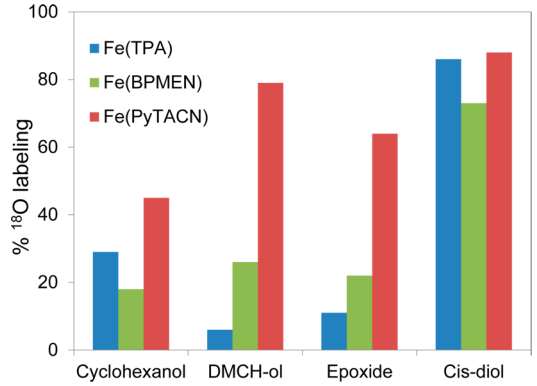

Figure 4. ^{18}O incorporation from 1000 equiv of added $H_2{}^{18}O$ into products of cyclohexane, *cis*-1,2-dimethylcyclohexane, and cyclooctene oxidation by iron catalysts using H_2O_2. The % *cis*-diol labeling corresponds to the amount of $^{16}O^{18}O$-*cis*-diol formed. Based on data from refs 17, 18, 26, and 27.

for all oxygenated products of reactions carried out using catalysts **1**, **2**, and **3**.[17,18,26,27] These results exclude the possibility of direct substrate oxidation by an iron−H_2O_2 adduct and require O−O bond cleavage to occur prior to substrate oxidation to allow added water to become incorporated into the metal-based oxidant. Interestingly, the % ^{18}O-labeling observed depends on the nature of the product and the catalyst used. For alcohol and epoxide products, partial label incorporation was observed, but nearly full incorporation of one ^{18}O atom from water was found for the *cis*-diol products. Furthermore, the % ^{18}O-incorporation was found to depend on the strength of the alkane C−H bond.[17] Lastly, in the case of **1**, the extent of ^{18}O-labeling increased with $H_2{}^{18}O$ concentration and displayed saturation behavior (Figure 5),[17,26,28] suggesting a water-binding pre-equilibrium that incorporates label from water into the metal-based intermediate prior to the substrate oxidation step.

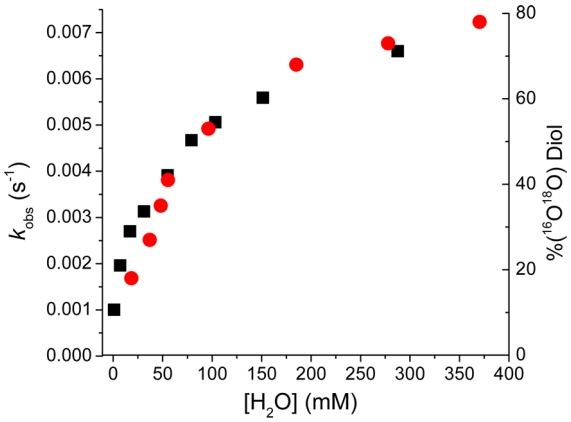

Figure 5. Water concentration dependence for the decay rate of **1a** at −40 °C (■) and the fraction of *cis*-diol with a single ^{18}O-label obtained in the oxidation of 1-octene by **1a** and H_2O_2 in the presence of $H_2{}^{18}O$ at 0 °C (●). Reproduced from ref 28. Copyright 2013 American Chemical Society.

DOI: 10.1021/acs.accounts.5b00053
Acc. Chem. Res. 2015, 48, 2612−2621

The above observations have led to the proposed mechanism presented in Scheme 2 that invokes formation of a Fe^{III}–OOH

Scheme 2. Proposed Mechanism of C=C and C–H Oxidation by Fe(II) Catalysts Supported by Tetradentate N4 Ligands That Accounts for the ^{18}O-Incorporation Patterns Observed for the Products Formed in the Presence of $H_2{}^{18}O$

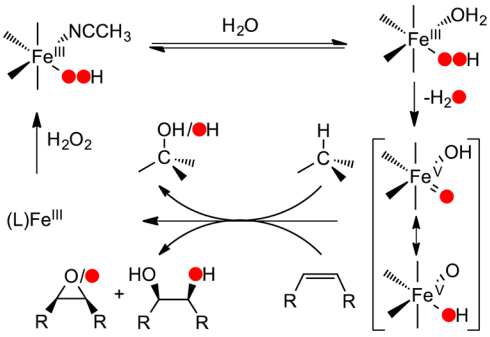

intermediate.[17,26] This intermediate undergoes water-assisted decay to afford a $Fe^{V}(O)(OH)$ species that is responsible for both C–H and C=C oxidation. In this scheme, the oxo and hydroxo ligands of the putative iron(V) oxidant derive from H_2O_2 and H_2O, respectively, so transfer of both oxygen atoms to an olefin substrate would yield a *cis*-diol product with one oxygen atom from H_2O_2 and the other from H_2O, as observed experimentally. Oxo-hydroxo tautomerism of the $Fe^{V}(O)(^{18}OH)$ species, first demonstrated by Meunier in synthetic oxometalloporhyrin complexes,[29] is invoked to rationalize the observed partial labeling of the monooxygenated epoxide and alcohol products, which varies with substrate and catalyst (Figure 4).[21,22,31,32] This variability reflects the relative rates of oxo–hydroxo tautomerization on the putative $Fe^{V}(O)(OH)$ oxidant and its attack of the substrate C–H or C=C bonds. The unusually high label incorporation found for the alcohol and epoxide products of **3**-catalyzed oxidations has been ascribed to steric factors that favor transfer of the water-derived O atom.[18,27,30]

THE METASTABLE Fe^{III}–OOH PRECURSOR TO A PUTATIVE $Fe^{V}(O)(OH)$ OXIDANT

Spectroscopic and kinetic studies have been carried out to test the mechanistic hypothesis proposed in Scheme 2. A transient purple intermediate, **1a**, was generated upon reacting a CH_3CN solution of catalyst **1** with excess H_2O_2 (30% w/w in H_2O) at −40 °C.[13,17,31] Intermediate **1a** exhibits a visible chromophore with λ_{max} = 538 nm (ε = 2200 $M^{-1}cm^{-1}$) and EPR signals at g = 2.19, 2.15, and 1.97 that are associated with an S = 1/2 iron(III) center (Figure 6, Table 1). The ESI-MS spectrum of **1a** showed a dominant peak at m/z 478 with a mass and an isotope distribution pattern fully consistent with its formulation as $[(TPA)Fe^{III}(OOH)ClO_4]^+$. Resonance Raman studies revealed enhanced vibrations at 624 and 803 cm^{-1}, which downshifted, respectively, by 19 and 44 cm^{-1} with the use of $H_2{}^{18}O_2$, allowing their assignment to ν(Fe–O) and ν(O–O) modes, respectively.[31] Thus, **1a** is identified as $[(TPA)Fe^{III}(OOH)(solv)]^{2+}$. Corresponding Fe^{III}–OOH intermediates with similar spectroscopic properties have been observed for iron(II) catalysts **2** and **4** (Table 1).

Kinetic studies were performed at −40 °C to establish the role of the $(L)Fe^{III}$–OOH intermediates in catalytic hydrocarbon oxidation reactions by the iron(II) catalysts.[28] The

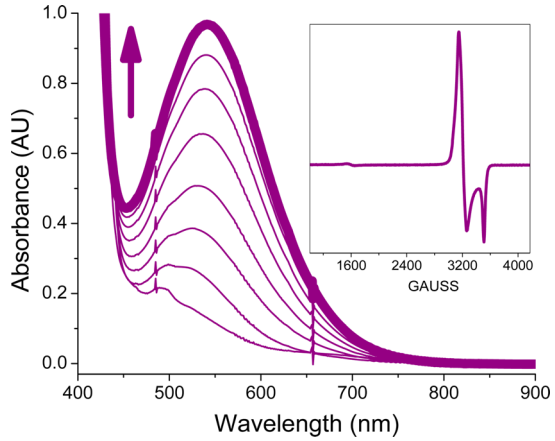

Figure 6. UV–visible spectral evolution of Fe^{III}–OOH intermediate **1a** upon addition of 10 equiv of H_2O_2 at −40 °C to 1 mM **1** in CH_3CN in the presence of 250 equiv of 1-octene. Inset: X-band EPR spectrum of **1a** in CH_3CN. Adapted from ref 13. Copyright 1997 American Chemical Society.

kinetic evolution of $(TPA)Fe^{III}$–OOH species **1a** in the presence of 1-octene was monitored by following the rise and fall of its visible chromophore as well as the appearance of 1,2-octanediol and 1,2-epoxyoctane products (Figure 7). Product formation commenced after a short lag phase during which **1a** accumulated. The lag phase was followed by a period of linear product formation during which time **1a** persisted in a pseudo-steady-state. Upon depletion of H_2O_2, **1a** decayed rapidly and product formation ceased. The decay rate of **1a** (k_{obs} = 0.0024(3) s^{-1}) was found to be comparable to the catalytic rate of product formation (k_{cat} = 0.0018(2) s^{-1}) under saturating 1-octene conditions. These observations show that **1a** is indeed on the path for **1**-catalyzed oxidation of 1-octene, undergoing rate-determining decay to unveil the species responsible for substrate oxidation.

Additional experiments shed further light on what factors control the rate-determining decay of the Fe^{III}–OOH intermediate. The **1a** decay rate was found to be independent of the nature of the added olefin and its concentration, emphasizing that there is no interaction between **1a** and the substrate. However, the presence of water made a difference. The decay rate of **1a** increased as a function of H_2O concentration and exhibited saturation behavior at high concentrations of added H_2O (Figure 5), providing kinetic evidence for a pre-equilibrium involving the binding of water to **1a** prior to its decay. Fitting this saturation plot to a one-site ligand binding function afforded an apparent association constant of 30 M^{-1}, a value in good agreement with those obtained from the labeling of 1,2-octanediol (30 M^{-1}),[26] 1,2-epoxyoctane (20 M^{-1}),[26] and cyclohexanol (16 M^{-1})[17] products as a function of $H_2{}^{18}O$ concentration. Furthermore, a kinetic isotope effect (KIE) of 2.5 was observed for both the decay of **1a** and the formation of 1,2-octanediol and 1,2-epoxyoctane products when parallel experiments were carried out in the presence of added H_2O or D_2O. These results indicate that the added H_2O aids in the proposed heterolytic cleavage of the O–O bond of **1a** to form the $Fe^{V}(O)(OH)$ oxidant (Scheme 2), where a proton on the metal-bound water hydrogen bonds to the distal O atom of the bound hydroperoxide to stabilize the incipient negative charge that forms on the leaving OH fragment. These observations reinforce lessons learned from studies of proton-facilitated

DOI: 10.1021/acs.accounts.5b00053
Acc. Chem. Res. 2015, 48, 2612–2621

Table 1. Spectroscopic Characterization of $S = 1/2$ Iron Species Observed in Nonheme Iron-Catalyzed Hydrocarbon Oxidation Reactions Using H_2O_2[a]

species	λ_{max} (ε_M)	EPR g values	% spin	proposed formulation	reaction conditions	ref
1a	538(2200)	2.19, 2.15, 1.97	45	(TPA)Fe^{III}–OOH	Fe^{II}(L)/H_2O_2/−40 °C	13,31
1a*	510(2200)	2.18, 2.15, 1.97	39	(TPA*)Fe^{III}–OOH	Fe^{II}(L)/H_2O_2/−40 °C	32
1b		2.71, 2.42, 1.53	7−15	(TPA)Fe^{V}=O	Fe^{II}(L)/RCO_3H/−60 °C	33,34
1b	460(4000)	2.71, 2.42, 1.53	21	(TPA)Fe^{III}–OOAc	Fe^{II}(L)/H_2O_2/AcOH/−40 °C	32
1b*	460(4000)	2.58, 2.42, 1.70	50	(TPA*)Fe^{III}–OOAc	Fe^{II}(L)/H_2O_2/AcOH/−40 °C	32
1c*		2.07, 2.01, 1.96	<3	(TPA*)Fe^{V}(O)(OAc)	Fe^{III}(L)/H_2O_2/AcOH/−80 °C	35
2a	560(1000)	2.21, 2.14, 1.96	25	(BPMEN)Fe^{III}–OOH	Fe^{II}(L)/H_2O_2/20 °C	34,36,37
2a*	560	2.20, 2.16, 1.95		(BPMEN*)Fe^{III}–OOH	Fe^{II}(L)/H_2O_2/0 °C	37
2b		2.69, 2.42, 1.70	8	(BPMEN)Fe^{V}=O	Fe^{II}(L)/H_2O_2/−70 °C	33,34
3b		2.66, 2.43, 1.74	3	(PyTACN)Fe^{V}=O	Fe^{II}(L)/H_2O_2/−70 °C	38
4a	560	2.20, 2.16, 1.96		(PDP)Fe^{III}–OOH	Fe^{II}(L)/H_2O_2/0 °C	23,37
4a*	560(1100)	2.22, 2.16, 1.96		(PDP*)Fe^{III}–OOH	Fe^{II}(L)/H_2O_2/−30 °C	37
4b		2.66, 2.42, 1.71		(PDP)Fe^{V}=O	Fe^{II}(L)/H_2O_2/−70 °C	23,35
4b*	465	2.72, 2.42	7	(PDP*)Fe^{III}(OOAc)	Fe^{II}(L)/H_2O_2/AcOH/−40 °C	37
4c*		2.07, 2.01, 1.96	1	(PDP*)Fe^{V}(O)(OAc)	Fe^{III}(L)/H_2O_2/AcOH/−80 °C	35

[a]See Chart 1 for ligand structures. All reactions at or above −40 °C were conducted in CH_3CN, while those below −40 °C were conducted in 1:2 v/v CH_3CN/CH_2Cl_2.

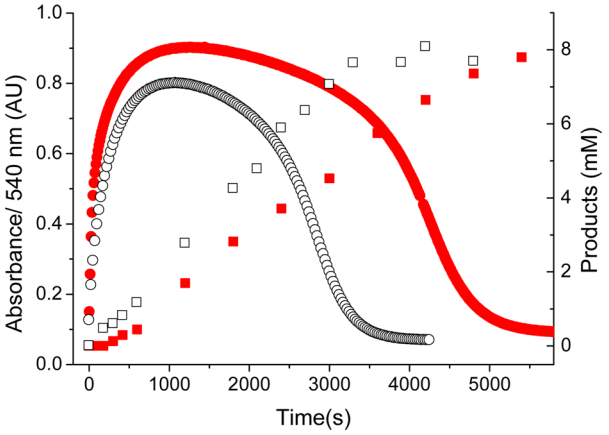

Figure 7. Time course for 1-octene (250 equiv) oxidation by 1 mM **1a** and 20 equiv of H_2O_2 in CH_3CN at −40 °C, monitored at 540 nm (●, ○) and by GC-determined amounts of olefin oxidation products (■, □). The reactions were conducted in the presence of 80 (red) or 116 (black) equiv of H_2O. Reproduced from ref 28. Copyright 2013 American Chemical Society.

O−O bond cleavage at the iron(III) centers of various enzymes.[39−42] Studies on the temperature dependence of **1a** decay yielded $\Delta H^{\ddagger}$ = 10.8(1) kcal/mol and $\Delta S^{\ddagger}$ = −23(3) cal/(mol K), which give a $\Delta G^{\ddagger}$ value at 298 K of 17.5(2) kcal/mol (Table S1). This value is in good agreement with the $\Delta G^{\ddagger}_{298}$ value of 19.2 kcal/mol calculated for the heterolytic O−O cleavage of **1a** by DFT.[43] In support of these mechanistic ideas, Costas and co-workers obtained variable temperature cryospray mass spectrometric evidence for an ion that corresponds to the putative Fe^{V}(O)(OH) species derived from catalyst **3** and showed that it is capable of olefin epoxidation and *cis*-dihydroxylation.[44] These results provide a solid foundation for the mechanism of C−H and C=C oxidation by (L)Fe^{II}/H_2O_2 proposed in Scheme 2.

THE REMARKABLE EFFECT OF A CARBOXYLIC ACID ADDITIVE

As first noted by White, Doyle, and Jacobsen in 2001,[45] the introduction of acetic acid into the Fe(L)/H_2O_2 reactions with olefins can increase both the yield and selectivity of the epoxide product. Importantly, carboxylic acid additives have led to the development of asymmetric epoxidation reactions, where quantitative product yields and enantioselectivities as high as 99% have been observed (Figure 3).[22−25] In a number of these transformations, the steric bulk of the carboxylic acid was found to influence the enantioselectivity of the epoxide product, where more sterically bulky acids led to higher % ee values.[23] Furthermore, White has shown that the introduction of acetic acid can enhance the selectivity and product yields of C−H activation reactions and facilitate the oxidation of specific C−H bonds in polyfunctional organic molecules with predictable selectivity (Figure 2).[19,20] These results demonstrate that the carboxylate moiety can significantly affect the selectivity-determining step of these reactions and therefore must be bound to the metal-based oxidant.

Subsequent efforts in the Que laboratory have focused on understanding the remarkable role the carboxylic acid additive plays in these iron-catalyzed oxidations. Studies of olefin oxidations by **1** and **2** showed that the selectivity for epoxide over *cis*-diol products increased upon AcOH addition.[46,47] Parallel to the effect of water discussed in the previous section, the decay rate of (TPA)Fe^{III}–OOH intermediate **1a** was enhanced upon AcOH addition[47] and exhibited an AcOH-concentration-dependent saturation behavior and an AcOH/AcOD kinetic isotope effect of 2. To accommodate increased selectivity for epoxide, the water-assisted mechanism shown in Scheme 2 evolved into the carboxylic-acid-assisted mechanism shown in Scheme 3, where a metal-bound carboxylic acid replaces the metal-bound water. Formation of the AcOH adduct was suggested by a change in the rhombic EPR spectrum of **1a** to an axial spectrum with g = 2.15, 2.15, and 1.97.[47] This adduct is proposed to undergo O−O bond heterolysis to generate a Fe^{V}(O)(O_2CR) oxidant, which would easily account for the high preference for epoxidation.[47] Additionally, under reaction conditions highly selective for cyclooctene epoxidation, there was a minor byproduct that was identified as *cis*-2-acetoxycyclooctanol, which could arise from the [3 + 2] addition of the proposed oxidant to the C=C bond of the olefin.[48,49]

DOI: 10.1021/acs.accounts.5b00053
Acc. Chem. Res. 2015, 48, 2612−2621

Scheme 3. Proposed Mechanism for C=C and C−H Oxidation by Nonheme Iron(II) Catalysts in the Presence of Carboxylic Acids

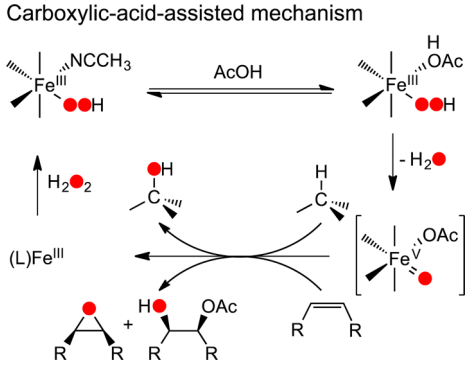

Low-temperature spectroscopic experiments were performed with the goal of trapping the proposed $Fe^{V}(O)(OAc)$ species. Talsi and co-workers identified an intermediate **1b** with a highly rhombic $S = 1/2$ EPR signal having g-values of 2.71, 2.42, and 1.53 ($g_{ave} = 2.22$, $\Delta g = 1.2$) from the reaction of **1** and either AcOOH or mCPBA in 1.7:1 CH_2Cl_2/MeCN at −70 °C (**1b**, Table 1).[33,34] This signal represented between 7% and 15% of the total Fe in the sample and underwent exponential decay at −70 °C. Although the rate of **1b** decay was not significantly affected by the addition of electron-deficient olefins, the addition of 12 equiv of cyclohexene did accelerate the decay process 5-fold and formed cyclohexene oxide in 80% yield. These results led to the proposed assignment of **1b** as the elusive Fe^{V}=O intermediate.

The resemblance of the g-values of **1b** to those associated with $S = 1/2$ iron(III) centers, together with the fact that the three Fe^{V}=O species characterized to date had smaller g_{ave} values (1.93−2.01) and much lower rhombicity ($\Delta g <$ 0.25),[50−52] raised doubts about this assignment. We thus sought to characterize this species by additional spectroscopic methods to ascertain the proposed iron(V) oxidation state. This task was however made challenging by the low percentage of **1b** generated in the samples.

In exploring variations of reaction conditions to increase the fraction of **1b** in the sample, we found that addition of excess AcOH to a CH_3CN solution of the Fe^{III}−OOH intermediate **1a** at −40 °C generated with 70% H_2O_2 (to limit the amount of water in the sample) gave rise to EPR signals very similar to those reported for **1b** by Talsi (Table 1).[32] These EPR signals were more intense (21%) than those obtained by Talsi[33,34] and could be associated with a visible chromophore at 460 nm ($\varepsilon_M \approx 4000$).[32]

Replacement of the TPA ligand with its more electron-donating TPA* analog (Chart 1) gave rise to an intermediate designated as **1b*** with sharper EPR signals at $g = 2.58$, 2.42, 1.70 from the reaction of $(TPA^*)Fe^{III}$−OOH (**1a***) and AcOH (Figure 8).[32] Species **1b*** also exhibited an intense chromophore at 460 nm that tracked the formation and decay of the $g_{max} = 2.58$ EPR signals (Figure S1). This species could also be generated in similar yields using **1***/AcOOH or **1***/*m*CPBA, combinations analogous to those used by Talsi to generate **1b**.[33,34] Importantly, the EPR signals of **1b*** represented almost half of the Fe in the sample, and its higher yield allowed its more detailed spectroscopic characterization that led us to formulate **1b*** as an acylperoxoiron(III) complex. Species **1b*** exhibits a dominant ESI-MS peak cluster at m/z =

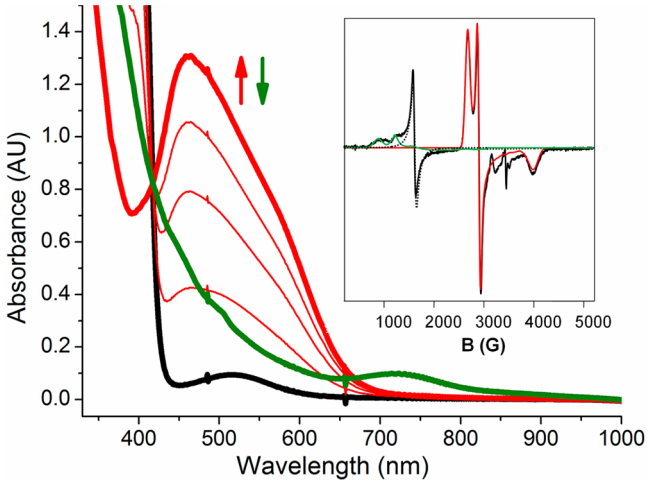

Figure 8. Spectral evolution of **1b*** (red) formed from 0.5 mM **1*** (black), 10 equiv of 70% H_2O_2, and 200 equiv of AcOH at −40 °C in CH_3CN. Inset: X-band EPR spectrum of **1b*** shown in red. Reproduced with permission from ref 32. Copyright 2014 Nature Publishing Group.

345.6167 for the intermediate derived from *m*CPBA. Resonance Raman studies revealed several enhanced vibrations that together could only arise from an acylperoxo ligand. Most importantly, Mössbauer studies revealed an iron center with a quadrupole splitting $\Delta E_Q = 2.60(5)$ mm/s and an isomer shift $\delta = +0.17(3)$ mm/s, parameters consistent only with an $S = 1/2$ iron(III) center. These values were well reproduced by DFT calculations on $[(TPA^*)Fe^{III}(\kappa^2\text{-}OOC(O)R)]^{2+}$ with the O atom of the terminal peroxo ligand bound *trans* to the TPA* amine donor (Figure 9).[32]

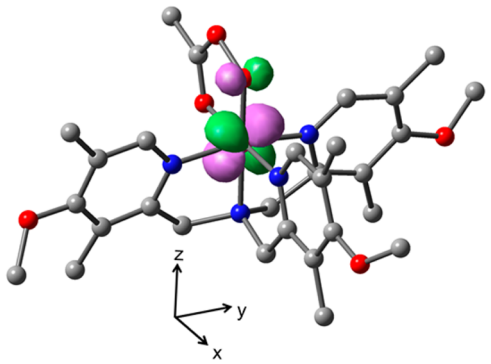

Figure 9. Geometry-optimized structure for **1b*** (Gaussian 09/B3LYP/6-311G). Reproduced with permission from ref 32. Copyright 2014 Nature Publishing Group.

Kinetic studies of **1b*** were conducted in the presence of 1-octene at −40 °C in order to determine how it is involved in olefin epoxidation. As illustrated in Figure 10, **1b*** rapidly formed upon addition of H_2O_2 to a CH_3CN mixture of **1***, AcOH, and 1-octene and then persisted in a pseudo-steady-state phase. Upon depletion of H_2O_2, **1b*** underwent exponential decay with a first order rate constant of 0.018(3) s^{-1}. GC product analysis of aliquots of the reaction mixture collected at various time points and quenched at −40 °C showed a linear formation of 1,2-epoxyoctane after a short lag phase ($v = 0.017(3)$ mM·s^{-1}), which ceased upon complete decay of **1b***, indicating that **1b*** is a catalytically competent

DOI: 10.1021/acs.accounts.5b00053
Acc. Chem. Res. 2015, 48, 2612−2621

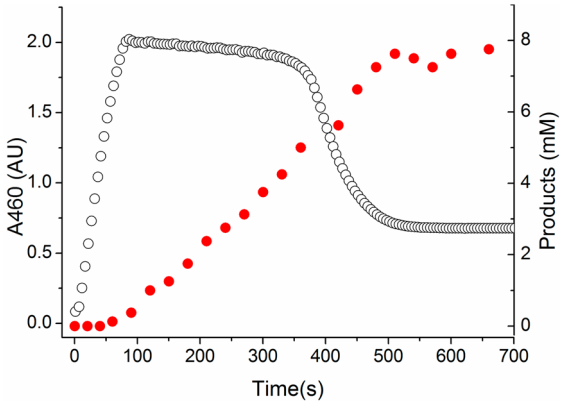

Figure 10. Monitoring the A460 value corresponding to **1b*** (○) as a function of time in the oxidation of 1-octene (250 equiv) with **1*** (1.0 mM) and 20 equiv of 70% H_2O_2 at −40 °C. Parallel monitoring of the epoxide product (●) by GC analysis of reaction aliquots quenched at −40 °C. Reproduced with permission from ref 32. Copyright 2014 Nature Publishing Group.

intermediate. Intermediate **1b*** decayed at a rate independent of the amount of substrate present (0−250 equiv) as well as the nature of the substrate (1-octene, cyclooctene, or 2-heptene), so **1b*** does not oxidize the substrate directly but must be converted into the actual oxidizing species, which we have proposed to be $Fe^{V}(O)(O_2CR)$ by analogy to the $Fe^{V}(O)$-(OH) oxidant in the water-assisted decay of **1a** discussed in an earlier section.

A comparison of the kinetic properties of **1a** and **1b*** shows that the latter is an order of magnitude more reactive at −40 °C (Table S1). Furthermore, **1b*** decay does not exhibit an AcOH/AcOD kinetic isotope effect (versus a H_2O/D_2O KIE of 2.5 for **1a** decay). Comparison of activation enthalpies and entropies for their exponential decay with those obtained for other peroxoiron(III) complexes in Table S1 shows that the activation parameters of **1a** are essentially identical to those of $[Fe^{III}(TMC)(OOH)]^{2+}$ in the presence of $HClO_4$, but **1b*** stands out among the entries in Table S1 with the highest activation enthalpy and a near-zero activation entropy. These observations suggest that **1a** and **1b*** likely decay via different pathways.

Upon standing in the absence of substrate, **1b*** decayed quantitatively to its $Fe^{IV}(O)$ derivative (Figure 8, green trace). A similar outcome was noted for **1a** but only in the presence of added carboxylic acid.[47] The observed conversion of the iron(III) centers of **1a** and **1b*** to oxoiron(IV) species is most easily rationalized by invoking homolytic cleavage of the O−O bonds of these peroxo intermediates and presumably forming a carboxyl radical ($RCOO^{\bullet}$) byproduct that in turn decomposes to CO_2 and $R^{\bullet}$. The fate of the incipient $R^{\bullet}$ moiety could be tracked in experiments with $PhCH_2COOH$ or C_6F_5COOH instead of acetic acid. In the C_6F_5COOH experiment, $C_6F_5^{\bullet}$ underwent rebound with the $Fe^{IV}(O)$ byproduct to form C_6F_5OH,[53,54] while the more stable benzyl radical formed in the $PhCH_2COOH$ experiment did not undergo rebound but was instead oxidized to benzaldehyde by O_2, allowing the $Fe^{IV}(O)$ coproduct to be observed at the end of the reaction.[47] In both cases, however, oxidative decarboxylation of the added RCOOH could be prevented by introducing an olefin, which was catalytically oxidized to epoxide. Thus, olefin epoxidation and oxidative decarboxylation of the carboxylic acid additive are competitive pathways that must diverge from a common intermediate.

These experimental results can be rationalized by a mechanism based on DFT calculations of Wang and Shaik on the fate of the spectroscopically characterized $(L)Fe^{III}(\kappa^2$-$OOC(O)R)$ intermediate **1b*** (Scheme 4).[32] They found that

Scheme 4. Mechanism for Olefin Oxidation by the Fe^{III}−OOC(O)R Intermediate 1b* Based on DFT Calculations of Wang and Shaik[32,55,a]

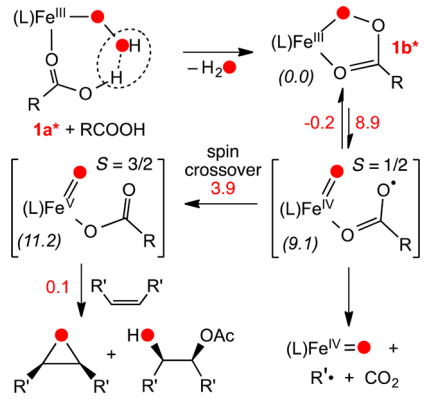

[a]Italicized numerical values are energies in kcal/mol calculated for the three electromers. Values in red adjacent to reaction arrows are calculated activation barriers in kcal/mol.

$S = 1/2$ **1b*** undergoes O−O bond lysis to form an $S = 1/2$ $Fe^{IV}(O)(^{\bullet}OC(O)R)$ species, which can in turn convert by spin crossover to an $S = 3/2$ $Fe^{V}(O)(OAc)$ electromer. The $S = 1/2$ $Fe^{IV}(O)(^{\bullet}OC(O)R)]$ electromer encounters a substantial barrier for olefin epoxidation and reverts readily to **1b***. In contrast, the $S = 3/2$ $Fe^{V}(O)(OAc)$ electromer epoxidizes olefins without a barrier, making it the likely epoxidizing agent. Talsi's observations that the enantioselectivity of olefin epoxidation reactions is dependent on the nature of the carboxylic acid additive also support the involvement of an $Fe^{V}(O)(OAc)$ oxidant.[23] On the other hand, the $S = 1/2$ $Fe^{IV}(O)(^{\bullet}OC(O)R)]$ electromer would account for the side reactions that involve loss of CO_2.

PERSPECTIVES

We have trapped and characterized at −40 °C in MeCN two distinct $S = 1/2$ iron(III)−peroxo intermediates involved in iron-catalyzed H_2O_2 activation by water-assisted or carboxylic-acid-assisted mechanisms. In the first case, we have identified **1a** as a hydroperoxoiron(III) species, which decays at a rate similar to that of product formation. Neither rate is affected by changing substrate concentration, but both are accelerated by water and exhibit an H_2O/D_2O KIE of 2.5.[28] Therefore, **1a** does not oxidize substrates directly but must first undergo a water-assisted, rate-determining O−O bond heterolysis to form a fleeting $Fe^{V}(O)(OH)$ oxidant evidenced only by cryospray ionization mass spectrometry;[44] the latter rationalizes the observed patterns for isotope incorporation from $H_2{}^{18}O$ into the various reaction products (Scheme 2).[17,18,26,27] In the second case where AcOH is present as an additive, we have characterized intermediate **1b***, which is best described as an acylperoxoiron(III) species.[32] Like **1a**, **1b*** does not oxidize the substrates directly but first undergoes O−O bond homolysis to afford an $Fe^{IV}(O)(OAc^{\bullet})$ species that can convert to its

DOI: 10.1021/acs.accounts.5b00053
Acc. Chem. Res. 2015, 48, 2612−2621

Table 2. SEPR *g*-values of Proposed or Established (L)Fe^{V}(O) or ($L^{\bullet}$)Fe^{IV}(O) Complexes[a]

	g values	g_{ave}	$g_{max} - g_{min}$	refs
1c*	2.070, 2.005, 1.956	2.010	0.114	35
4c*	2.071, 2.008, 1.960	2.013	0.111	35
$[(TMC)Fe(O)(NR)]^{+}$	2.05, 2.01, 1.97	2.01	0.08	52
$[(TAML)Fe(O)]^{-}$	1.99, 1.97, 1.74	1.90	0.25	50,51
$[(Me_3TACN)Fe(O)$-(3-Cl-acac)$]^{2+}$	1.97, 1.93, 1.91	1.94	0.06	56
$[(TBP_8Cz)Fe(O)]$	2.09, 2.05. 2.02	2.05	0.07	57
CYP119 Cpd I	2.00, 1.96, 1.86	1.94	0.14	8

[a]Abbreviations used: TMC = tetramethylcyclam; TAML = tetraanionic macrocyclic ligand; Me_3TACN = 1,4,7-trimethyl-1,4,7-triazacyclononane; Cl-acac = 3-chloroacetylacetonate; TBP_8Cz = octakis(4-*tert*-butylphenyl)corrolazine trianion.

Fe^{V}(O)(OAc) valence tautomer. The latter epoxidizes olefins, while the former accounts for oxidative decarboxylation byproducts that form in competition with olefin epoxidation.

The reaction landscape we have described thus far is based on only our observations on **1a** and **1b***, intermediates that represent the major iron components in the samples studied and are thus amenable to detailed spectroscopic characterization and kinetic analysis. However, this mechanistic picture is clearly far from being complete, and there remain questions raised by EPR studies in CH_3CN/CH_2Cl_2 at −60 °C or below (Table 1).[23,33,34,38] Under these reaction conditions, the decay rate of the highly rhombic g_{max} = 2.7 EPR signal assigned to **1b** was accelerated 5-fold upon addition of 12 equiv of cyclohexene, suggesting a direct involvement of **1b** in cyclohexene oxidation. Furthermore, similarly rhombic EPR signals were observed in the reactions of H_2O_2 with **2**, **3**, or **4** in the absence of added AcOH (Table 1),[23,33,34,38] which argue against an assignment of these EPR-active intermediates to acylperoxoiron(III) species as in the case of **1b***. These apparent inconsistencies remain to be clarified.

A highly relevant new result was reported while this manuscript was under review. New EPR signals with *g* = 2.07, 2.01, and 1.96 were observed in reaction mixtures of diferric complexes of TPA* or PDP* with H_2O_2 and AcOH in CH_3CN/CH_2Cl_2 at −80 °C (Table 1, **1c*** and **4c***).[35] Interestingly, the EPR properties of the new signals resemble those of the three bona fide oxoiron(V) complexes characterized thus far,[50−52] namely $[(TAML)Fe^{V}(O)]^{-}$ and $[(TMC)Fe^{V}(O)(NR)]^{+}$, and of species either proposed or shown to be oxoiron(IV)−ligand radical complexes (Table 2).[56,57] The authors propose these new *S* = 1/2 species as having either (L)Fe^{V}(O) or ($L^{\bullet}$)Fe^{IV}(O) centers, but the low yields of 2−3% make it very difficult to establish the iron oxidation states of these novel species.

Lastly, DFT calculations by Wang and Shaik support the likely involvement of (L)Fe^{V}(O) or ($L^{\bullet}$)Fe^{IV}(O) species.[32] These studies revealed a rather flat reaction surface involving three electromers, namely, (L)Fe^{III}(κ^2-OOC(O)R), Fe^{IV}(O)-($^{\bullet}$OC(O)R), and Fe^{V}(O)(OAc), that are connected by relatively small energy barriers (Scheme 4). Thus, a change in supporting ligand or reaction conditions may alter their relative energetics to allow the observation of any of these possible intermediates. Further studies on intermediates derived from iron catalysts supported by other ligands should provide a better definition of this fascinating reaction landscape.

■ ASSOCIATED CONTENT

Supporting Information

The Supporting Information is available free of charge on the ACS Publications website at DOI: 10.1021/acs.accounts.5b00053.

Eyring activation parameters for the decay of Fe^{III}−OOR complexes (Table S1) and time course of **1b*** and the Fe^{IV}=O decay product (Figure S1) (PDF)

■ AUTHOR INFORMATION

Funding

This work was supported by the US Department of Energy, Office of Basic Energy Sciences (Grant DE-FG02-03ER15455 to L.Q.)

Notes

The authors declare no competing financial interest.

Biographies

Williamson Oloo received his Ph.D. in the area of organometallic chemistry from the University of Maryland in 2011 under the direction of Andrei Vedernikov. He is currently a postdoctoral associate at the University of Minnesota and working with Professor Que on developing bioinspired iron catalysts for hydrocarbon oxidation reactions.

Larry Que obtained his Ph.D. from the University of Minnesota in 1973 and is currently Regents Professor at the University of Minnesota. His long-term research interests have focused on how biological nonheme iron centers activate dioxygen to carry out an amazing array of oxidative transformations. Larry's achievements in biomimetic nonheme iron chemistry have been recognized by the Frontiers in Biological Chemistry Award from the Max-Planck-Institut für Bioanorganishe Chemie (2005), the ACS Alfred Bader Award in Bioorganic or Bioinorganic Chemistry (2008), the RSC Inorganic Reaction Mechanisms Award (2011), the John C. Bailar, Jr. Medal (2012), and the JSCC International Award (2015).

■ REFERENCES

(1) Costas, M.; Mehn, M. P.; Jensen, M. P.; Que, L., Jr. Dioxygen activation at mononuclear nonheme iron active sites: Enzymes, models, and intermediates. *Chem. Rev.* **2004**, *104*, 939−986.
(2) Krebs, C.; Fujimori, D. G.; Walsh, C. T.; Bollinger, J. M. Non-heme Fe(IV)-oxo intermediates. *Acc. Chem. Res.* **2007**, *40*, 484−492.
(3) Barry, S. M.; Challis, G. L. Mechanism and catalytic diversity of Rieske non-heme iron- dependent oxygenases. *ACS Catal.* **2013**, *3*, 2362−2370.
(4) Denisov, I. G.; Makris, T. M.; Sligar, S. G.; Schlichting, I. Structure and chemistry of cytochrome P450. *Chem. Rev.* **2005**, *105*, 2253−2277.

DOI: 10.1021/acs.accounts.5b00053
Acc. Chem. Res. 2015, 48, 2612−2621

(5) Karlsson, A.; Parales, J. V.; Parales, R. E.; Gibson, D. T.; Eklund, H.; Ramaswamy, S. Crystal structure of naphthalene dioxygenase: Side-on binding of dioxygen to iron. *Science* **2003**, *299*, 1039−1042.
(6) Ashikawa, Y.; Fujimoto, Z.; Usami, Y.; Inoue, K.; Noguchi, H.; Yamane, H.; Nojiri, H. Structural insight into the substrate- and dioxygen-binding manner in the catalytic cycle of Rieske nonheme iron oxygenase system, carbazole 1,9a-dioxygenase. *BMC Struct. Biol.* **2012**, *12*, 15.
(7) Neibergall, M. B.; Stubna, A.; Mekmouche, Y.; Münck, E.; Lipscomb, J. D. Hydrogen peroxide dependent cis-dihydroxylation of benzoate by fully oxidized benzoate 1,2-dioxygenase. *Biochemistry* **2007**, *46*, 8004−8016.
(8) Rittle, J.; Green, M. T. Cytochrome P450 compound I: capture, characterization, and C-H bond activation kinetics. *Science* **2010**, *330*, 933−937.
(9) Wolfe, M. D.; Lipscomb, J. D. Hydrogen peroxide-coupled cis-diol formation catalyzed by naphthalene 1,2-dioxygenase. *J. Biol. Chem.* **2003**, *278*, 829−835.
(10) Wackett, L. P.; Kwart, L. D.; Gibson, D. T. Benzylic monooxygenation catalyzed by toluene dioxygenase from Pseudomonas putida. *Biochemistry* **1988**, *27*, 1360−1367.
(11) Que, L., Jr.; Tolman, W. B. Biologically inspired oxidation catalysis. *Nature* **2008**, *455*, 333−340.
(12) Costas, M.; Chen, K.; Que, L., Jr. Biomimetic nonheme iron catalysts for alkane hydroxylation. *Coord. Chem. Rev.* **2000**, *200-202*, 517−544.
(13) Kim, C.; Chen, K.; Kim, J. H.; Que, L., Jr. Stereospecific alkane hydroxylation with H_2O_2 catalyzed by an iron(II)-tris(2-pyridylmethyl)amine complex. *J. Am. Chem. Soc.* **1997**, *119*, 5964−5965.
(14) Sun, C.-L.; Li, B.-J.; Shi, Z.-J. Direct C-H transformation via iron catalysis. *Chem. Rev.* **2011**, *111*, 1293−1314.
(15) Oloo, W. N.; Que, L., Jr. Hydrocarbon oxidations catalyzed by bio-inspired nonheme iron and copper catalysts. In *Comprehensive Inorganic Chemistry II*; Reedijk, J., Poeppelmeier, K., Eds.; Elsevier: Oxford, U.K., 2013; Vol. *6*, pp 763−778.
(16) Bryliakov, K. P.; Talsi, E. P. Active sites and mechanisms of bioinspired oxidation with H_2O_2, catalyzed by non-heme Fe and related Mn complexes. *Coord. Chem. Rev.* **2014**, *276*, 73−96.
(17) Chen, K.; Que, L., Jr. Stereospecific Alkane Hydroxylation by Nonheme Iron Catalysts: Mechanistic Evidence for an Fe^V = O Active Species. *J. Am. Chem. Soc.* **2001**, *123*, 6327−6337.
(18) Company, A.; Gomez, L.; Guell, M.; Ribas, X.; Luis, J. M.; Que, L., Jr.; Costas, M. Alkane hydroxylation by a nonheme iron catalyst that challenges the heme paradigm for oxygenase action. *J. Am. Chem. Soc.* **2007**, *129*, 15766−15767.
(19) Chen, M. S.; White, M. C. A predictably selective aliphatic C-H oxidation reaction for complex molecule synthesis. *Science* **2007**, *318*, 783−787.
(20) Chen, M. S.; White, M. C. Combined effects on selectivity in Fe-catalyzed methylene oxidation. *Science* **2010**, *327*, 566−571.
(21) Gelalcha, F. G. Biomimetic iron-catalyzed asymmetric epoxidations: Fundamental concepts, challenges and opportunities. *Adv. Synth. Catal.* **2014**, *356*, 261−299.
(22) Cussó, O.; Ribas, X.; Lloret-Fillol, J.; Costas, M. Synergistic interplay of a non-heme iron catalyst and amino acid coligands in H_2O_2 activation for asymmetric epoxidation of alpha-alkyl-substituted styrenes. *Angew. Chem., Int. Ed.* **2015**, *54*, 2729−2733.
(23) Lyakin, O. Y.; Ottenbacher, R. V.; Bryliakov, K. P.; Talsi, E. P. Asymmetric epoxidations with H_2O_2 on Fe and Mn aminopyridine catalysts: Probing the nature of active species by combined electron paramagnetic resonance and enantioselectivity study. *ACS Catal.* **2012**, *2*, 1196−1202.
(24) Wang, B.; Wang, S.; Xia, C.; Sun, W. Highly enantioselective epoxidation of multisubstituted enones catalyzed by non-heme iron catalysts. *Chem. - Eur. J.* **2012**, *18*, 7332−7335.
(25) Cussó, O.; Garcia-Bosch, I.; Ribas, X.; Lloret-Fillol, J.; Costas, M. Asymmetric epoxidation with H_2O_2 by manipulating the electronic properties of non-heme iron catalysts. *J. Am. Chem. Soc.* **2013**, *135*, 14871−14878.
(26) Chen, K.; Costas, M.; Kim, J.; Tipton, A. K.; Que, L., Jr. Olefin cis-dihydroxylation versus epoxidation by nonheme iron catalysts: Two faces of an Fe^{III}-OOH coin. *J. Am. Chem. Soc.* **2002**, *124*, 3026−3035.
(27) Company, A.; Feng, Y.; Güell, M.; Ribas, X.; Luis, J. M.; Que, L., Jr.; Costas, M. Olefin-Dependent discrimination between two nonheme HO-Fe^V = O tautomeric species in catalytic H_2O_2 epoxidations. *Chem. - Eur. J.* **2009**, *15*, 3359−3362.
(28) Oloo, W. N.; Fielding, A. J.; Que, L., Jr. Rate determining water-assisted O−O bond cleavage of a Fe^{III}−OOH intermediate in a bio-inspired nonheme iron-catalyzed oxidation. *J. Am. Chem. Soc.* **2013**, *135*, 6438−6441.
(29) Meunier, B.; Bernadou, J. Active iron-oxo and iron-peroxo species in cytochromes P450 and peroxidases; oxo-hydroxo tautomerism with water-soluble metalloporphyrins. *Struct. Bonding (Berlin)* **2000**, *97*, 1−35.
(30) Mitra, M.; Lloret-Fillol, J.; Haukka, M.; Costas, M.; Nordlander, E. Evidence that steric factors modulate reactivity of tautomeric iron-oxo species in stereospecific alkane C-H hydroxylation. *Chem. Commun.* **2014**, *50*, 1408−1410.
(31) Mairata i Payeras, A.; Ho, R. Y. N.; Fujita, M.; Que, L., Jr. The reaction of [Fe^{II}(tpa)] with H_2O_2 in acetonitrile and acetone-distinct intermediates and yet similar catalysis. *Chem. - Eur. J.* **2004**, *10*, 4944−4953.
(32) Oloo, W. N.; Meier, K. K.; Wang, Y.; Shaik, S.; Münck, E.; Que, L., Jr. Identification of a low-spin acylperoxoiron(III) intermediate in bio-inspired nonheme iron-catalyzed oxidations. *Nat. Commun.* **2014**, *5*, 3046.
(33) Lyakin, O. Y.; Bryliakov, K. P.; Britovsek, G. J.; Talsi, E. P. EPR spectroscopic trapping of the active species of nonheme iron-catalyzed oxidation. *J. Am. Chem. Soc.* **2009**, *131*, 10798−10799.
(34) Lyakin, O. Y.; Bryliakov, K. P.; Talsi, E. P. EPR, ^1H and ^2H NMR, and reactivity studies of the iron oxygen intermediates in bioinspired catalyst systems. *Inorg. Chem.* **2011**, *50*, 5526−5538.
(35) Lyakin, O. Y.; Zima, A. M.; Samsonenko, D. G.; Bryliakov, K. P.; Talsi, E. P. EPR spectroscopic detection of the elusive Fe^V = O intermediates in selective catalytic oxofunctionalizations of hydrocarbons mediated by biomimetic ferric complexes. *ACS Catal.* **2015**, *5*, 2702−2707.
(36) Makhlynets, O. V.; Rybak-Akimova, E. V. Aromatic hydroxylation at a non-heme iron center: Observed intermediates and insights into the nature of the active species. *Chem. - Eur. J.* **2010**, *16*, 13995−14006.
(37) Makhlynets, O. V.; Oloo, W. N.; Moroz, Y. S.; Belaya, I. G.; Palluccio, T. D.; Filatov, A. S.; Müller, P.; Cranswick, M. A.; Que, L., Jr.; Rybak-Akimova, E. V. H_2O_2 activation with biomimetic non-haem iron complexes and AcOH: connecting the g = 2.7 EPR signal with a visible chromophore. *Chem. Commun.* **2014**, *50*, 645−648.
(38) Lyakin, O. Y.; Prat, I.; Bryliakov, K. P.; Costas, M.; Talsi, E. P. EPR detection of Fe(V) = O active species in nonheme iron-catalyzed oxidations. *Catal. Commun.* **2012**, *29*, 105−108.
(39) Dunford, H. B.; Hewson, W. D.; Steiner, H. Horseradish peroxidase. XXIX. Reactions in water and deuterium oxide: cyanide binding, compound I formation, and reactions of compounds I and II with ferrocyanide. *Can. J. Chem.* **1978**, *56*, 2844−2852.
(40) Aikens, J.; Sligar, S. G. Kinetic solvent isotope effects during oxygen activation by cytochrome P-450cam. *J. Am. Chem. Soc.* **1994**, *116*, 1143−1144.
(41) Lee, S. Y.; Lipscomb, J. D. Oxygen activation catalyzed by methane monooxygenase hydroxylase component: Proton delivery during the O-O bond cleavage steps. *Biochemistry* **1999**, *38*, 4423−4432.
(42) Tinberg, C. E.; Lippard, S. J. Revisiting the mechanism of dioxygen activation in soluble methane monooxygenase from M. capsulatus (bath): Evidence for a multi-step, proton-dependent reaction pathway. *Biochemistry* **2009**, *48*, 12145−12158.
(43) Bassan, A.; Blomberg, M. R. A.; Siegbahn, P. E. M.; Que, L., Jr. A density functional study of O-O bond cleavage for a biomimetic

DOI: 10.1021/acs.accounts.5b00053
Acc. Chem. Res. 2015, 48, 2612−2621

non-heme iron complex demonstrating an Fe^{V} intermediate. *J. Am. Chem. Soc.* **2002**, *124*, 11056−11063.
(44) Prat, I.; Mathieson, J. S.; Guell, M.; Ribas, X.; Luis, J. M.; Cronin, L.; Costas, M. Observation of Fe(v) = O using variable-temperature mass spectrometry and its enzyme-like C-H and C═C oxidation reactions. *Nat. Chem.* **2011**, *3*, 788−793.
(45) White, M. C.; Doyle, A. G.; Jacobsen, E. N. A synthetically useful, self-assembling MMO mimic system for catalytic alkene epoxidation with aqueous H_2O_2. *J. Am. Chem. Soc.* **2001**, *123*, 7194−7195.
(46) Fujita, M.; Que, L., Jr. In situ formation of peracetic acid in iron-catalyzed epoxidations by hydrogen peroxide in the presence of acetic acid. *Adv. Synth. Catal.* **2004**, *346*, 190−194.
(47) Mas-Ballesté, R.; Que, L., Jr. Iron-catalyzed olefin epoxidation in the presence of acetic acid: Insights into the nature of the metal-based oxidant. *J. Am. Chem. Soc.* **2007**, *129*, 15964−15972.
(48) Mas-Ballesté, R.; Fujita, M.; Que, L., Jr. High-valent iron-mediated cis-hydroxyacetoxylation of olefins. *Dalton Trans.* **2008**, 1828−1830.
(49) Iyer, S. R.; Javadi, M. M.; Feng, Y.; Hyun, M. Y.; Oloo, W. N.; Kim, C.; Que, L., Jr. A chameleon catalyst for nonheme iron-promoted olefin oxidation. *Chem. Commun.* **2014**, *50*, 13777−13780.
(50) de Oliveira, F. T.; Chanda, A.; Banerjee, D.; Shan, X.; Mondal, S.; Que, L., Jr.; Bominaar, E. L.; Munck, E.; Collins, T. J. Chemical and spectroscopic evidence for an Fe^{V}-oxo complex. *Science* **2007**, *315*, 835−838.
(51) Ghosh, M.; Singh, K. K.; Panda, C.; Weitz, A.; Hendrich, M. P.; Collins, T. J.; Dhar, B. B.; Sen Gupta, S. Formation of a room temperature stable $Fe^{V}(O)$ complex: reactivity toward unactivated C-H bonds. *J. Am. Chem. Soc.* **2014**, *136*, 9524−9527.
(52) Van Heuvelen, K. M.; Fiedler, A. T.; Shan, X.; De Hont, R. H.; Meier, K. K.; Bominaar, E. L.; Münck, E.; Que, L., Jr. One-electron oxidation of an oxoiron(IV) complex to form an $[O = Fe^{V} = NR]^{+}$ center. *Proc. Natl. Acad. Sci. U. S. A.* **2012**, *109*, 11933−11938.
(53) Makhlynets, O. V.; Das, P.; Taktak, S.; Flook, M.; Mas-Ballesté, R.; Rybak-Akimova, E. V.; Que, L., Jr. Iron-promoted ortho- and/or ipso-hydroxylation of benzoic acids with H_2O_2. *Chem. - Eur. J.* **2009**, *15*, 13171−13180.
(54) Das, P.; Que, L., Jr. Iron catalyzed competitive olefin oxidation and ipso-hydroxylation of benzoic acids: Further evidence for an Fe^{V} = O oxidant. *Inorg. Chem.* **2010**, *49*, 9479−9485.
(55) Wang, Y.; Janardanan, D.; Usharani, D.; Han, K.; Que, L., Jr.; Shaik, S. Nonheme Iron Oxidant Formed in the Presence of H_2O_2 and Acetic Acid Is the Cyclic Ferric Peracetate Complex, Not a Perferryloxo Complex. *ACS Catal.* **2013**, *3*, 1334−1341.
(56) Tse, C. W.; Chow, T. W. S.; Guo, Z.; Lee, H. K.; Huang, J. S.; Che, C. M. Nonheme iron mediated oxidation of light alkanes with oxone: Characterization of reactive oxoiron(IV) ligand cation radical intermediates by spectroscopic studies and DFT calculations. *Angew. Chem., Int. Ed.* **2014**, *53*, 798−803.
(57) McGown, A. J.; Kerber, W. D.; Fujii, H.; Goldberg, D. P. Catalytic reactivity of a meso-N-substituted corrole and evidence for a high-valent iron−oxo species. *J. Am. Chem. Soc.* **2009**, *131*, 8040−8048.

DOI: 10.1021/acs.accounts.5b00053
Acc. Chem. Res. 2015, 48, 2612−2621